*J. Fluid Mech.* (1992), *vol.* 242, *pp.* 529–547
*Printed in Great Britain*



# Instabilities of three-dimensional viscous falling films

By S. W. JOO† AND S. H. DAVIS

Department of Engineering Sciences and Applied Mathematics, Northwestern University, Evanston, IL 60208, USA

(Received 11 June 1991 and in revised form 12 February 1992)

A long-wave evolution equation is used to study a falling film on a vertical plate. For certain wavenumbers there exists a two-dimensional strongly nonlinear permanent wave. A new secondary instability is identified in which the three-dimensional disturbance is spatially synchronous with the two-dimensional wave. The instability grows for sufficiently small cross-stream wavenumbers and does not require a threshold amplitude; the two-dimensional wave is always unstable. In addition, the nonlinear evolution of three-dimensional layers is studied by posing various initial-value problems and numerically integrating the long-wave evolution equation.

## 1. Introduction

A thin liquid layer flowing down an incline under the action of gravity is unstable to long-wave disturbances on the free surface. This surface-wave instability has been studied intensively since the early works of Yih (1955, 1963) and Benjamin (1957), as summarized by Lin (1983) and Lin & Wang (1985). Linear analyses show that the instability occurs for sufficiently long waves; i.e. there is a cutoff wavenumber beyond which the instability disappears. A number of weakly nonlinear analyses have been performed by Lin (1969), Gjevik (1970), and Pumir, Manneville & Pomeau (1983) among others, and these show nonlinear equilibration of initial unstable waves with wavenumbers near the cutoff value. The resulting finite-amplitude permanent waves are almost monochromatic when the initial wavenumber is very close to the cutoff value and become broader banded as the wavenumber is decreased toward longer waves. Lin (1974) studied the stability of the monochromatic permanent waves and showed that they are stable to sideband disturbances of Benjamin–Feir type. The full nonlinear behaviour of unstable layers including those with wavenumbers much smaller than the cutoff value has been studied (e.g. Pumir *et al.* 1983 and Joo, Davis & Bankoff, 1991) by numerically analyzing the long-wave evolution equation of Benney type (1966).

Some three-dimensional extensions of the aforementioned two-dimensional (no spanwise variation) studies have been done. Roskes (1970) generalized Benney's evolution equation to three dimensions, and Krishna & Lin (1977) generalized Lin's earlier stability analysis of two-dimensional monochromatic permanent waves to three-dimensional waves. Krishna & Lin, however, considered only oblique waves. As pointed out by Roskes (1970), an oblique wave is equivalent to a two-dimensional wave in rotated coordinates. The study of Krishna & Lin thus can be considered as a two-dimensional analysis in a non-optimal coordinate system. Surprisingly little

† Current address: Department of Mechanical Engineering, Wayne State University, Detroit, MI 48202, USA.

has been reported on the numerical study of three-dimensional layers. Melkonian & Maslowe (1990) have integrated a simplified evolution equation and examined the evolution of a three-dimensional localized wave. They assumed that the characteristic length in the spanwise direction is much shorter than that in the streamwise direction, and thus retained a spanwise dispersion effect in the lowest approximation for small surface slope. However, they neglected the higher-order correction and consequently the destabilizing mean-flow and the stabilizing capillary effects. The evolution does not involve any instability and shows monotonic flattening of the initial disturbance.

Experimental studies of falling films have been done by, among others, Kapitza & Kapitza (1949), Krantz & Goren (1971), Portalski & Clegg (1972), Alekseenko, Nakoryakov & Pokusaev (1985), and Lacy, Sheintuch & Dukler (1991). As summarized by Alekseenko *et al.*, in most of the experiments performed, two-dimensional regular waves are observed only near the wave-inception line. The waves soon become three-dimensional and irregular. In order to obtain two-dimensional wavetrains, the flow was disturbed at a fixed frequency by, for example, wire vibrations (Krantz & Goren) and pulsations of the flow rate (Kapitza & Kapitza and Alekseenko *et al.*).

In the present study, we discuss the dynamics of three-dimensional layers as described by the evolution equation. In particular, we report a new secondary instability of the two-dimensional permanent waves; the two-dimensional finite-amplitude waves are unstable to infinitesimal three-dimensional disturbances. This instability may be responsible for the three-dimensional wave development observed in experiments. For vertical plates, the instability does not require a threshold amplitude of the two-dimensional waves and gives rise to a short-wave cutoff in the spanwise direction due to the capillarity. Although the physical mechanisms are different, the instability is analogous to the secondary instability of the Tollmien–Schlichting waves in wall-bounded shear flows as described by Orszag & Patera (1983) and Herbert (1983). As did Orszag & Patera, we can examine the instability process in three steps: (i) primary linear instability on the undisturbed surface; (ii) nonlinear equilibration of primary instability into two-dimensional finite-amplitude permanent waves; (iii) secondary (three-dimensional) instability of the two-dimensional wave.

In the case of wall-bounded shear flows, there is a threshold amplitude for the three-dimensional instability and when it arises it does so on the rapid convective timescale. In the present thin-layer flows, the instability is unconditional (at least for vertical layers), restricted to long waves, and viscous in nature, as is the primary instability.

In §2, we review the primary instability and the nonlinear saturation. The finite-amplitude permanent waves are obtained by following the weakly nonlinear analysis of Gjevik (1970) and compared with nonlinear computations. In §3, we identify the secondary instability by a linear analysis. In §4, the instability is studied further by posing various initial-value problems in three dimensions and integrating numerically the strongly nonlinear evolution equation. Finally, in §5 we conclude by summarizing the results and discussing the new instability in relation to others known in the literature.

## 2. Primary instability and nonlinear saturation

A three-dimensional Newtonian liquid of constant density $\rho$ and viscosity $\mu$ is flowing down a vertical plane due to gravity. The liquid layer has a mean thickness of $d_0$, and is bounded by an interface with a passive gas. The characteristic length $l$ in the streamwise or spanwise direction (proportional to a typical wavelength of the interface) is much larger than $d_0$, and thus the long-wave asymptotics proposed by Benney (1966) allows description of the flow development. The full system of governing equation and boundary conditions than can be reduced into a single evolution equation for the local layer thickness $h(x, y, t)$:

$$h_t + Gh^2h_x + \epsilon\left[\frac{2G^2}{15}(h^6h_x)_x + S\nabla\cdot(h^3\nabla\nabla^2h)\right] + O(\epsilon^2) = 0 \tag{2.1}$$

(Krishna & Lin 1977), where $x$ and $y$ are, respectively, streamwise and spanwise coordinates, and $\nabla$ is the gradient operator $(\partial_x, \partial_y)$. Here, $h$, the spatial coordinates, and $t$ are scaled by $d_0$, $d_0/\epsilon$, and $\rho d_0^2/(\epsilon\mu)$, respectively, where $\epsilon = d_0/l \ll 1$. In (2.1), the Reynolds number is $G$,

$$G = \frac{\rho^2 d_0^3 g}{\mu^2}, \tag{2.2}$$

where $g$ is the gravitational acceleration, and the surface tension $\gamma$ is measured by

$$S = \epsilon^2\frac{\rho\gamma d_0}{3\mu^2}. \tag{2.3}$$

If one wishes to isolate $d_0$ in $G$ and obtain a measure of $\gamma$ independent of $d_0$, then one may replace $S$ by $T$,

$$S = TG^{\frac{1}{3}}. \tag{2.4}$$

The second term in (2.1) describes the wave propagation. The term is nonlinear, and so describes local steepening of disturbance waves. The third term (or the first term in the square bracket) in (2.1) describes the mean flow, and is responsible for the surface-wave instability. The fourth term describes the stabilizing capillary effects.

### 2.1. *Primary instability*

The basic state for the primary instability is a uniform undisturbed state $h = 1$, and the stability analysis proceeds by imposing an infinitesimal harmonic disturbance with the wavenumber vector $\boldsymbol{k} = (k\cos\theta, k\sin\theta)$ on the $(x, y)$-plane. Equation (2.1) allows normal-mode representation for the disturbance, and the linearized phase speed $c_{\mathrm{L}}$ and the linear growth rate $\Gamma$ are found to be

$$c_{\mathrm{L}} = \mathrm{G}, \tag{2.5}$$

$$\Gamma = \epsilon k^2\left(\frac{2G^2}{15}\cos^2\theta - Sk^2\right), \tag{2.6}$$

which clearly shows that for a given $k$ two-dimensional transverse waves ($\theta = 0$) are the preferred mode. Even for an oblique wave ($\theta \neq 0$), Roskes (1970) pointed out that (2.1) can be reduced to two dimensions by a simple coordinate rotation, or by replacing $G\cos\theta$ with $G'$ and setting $\partial_y = 0$. Therefore, we set $\theta = 0$, and concentrate on two-dimensional waves throughout this section. Since there is no hydrostatic

effect on vertical layers, the critical value of $G$ is zero and surface waves will grow for all values of $G$ as long as the disturbance wavenumber is smaller than the cutoff value $k_c = [2G^2/(15S)]^{\frac{1}{2}}$. A maximum linear growth rate occurs at $k = k_M = k_c/\sqrt{2}$.

The nature of the primary surface-wave instability can be studied by adopting the absolute/convective instability concepts, summarized by Huerre & Monkewitz (1990). In convectively unstable flows, the growing disturbance wave moves away from its source, whereas in absolutely unstable flows, the instability contaminates the entire flow field. We follow the analysis of Deissler (1987) applied to a plane Poiseuille flow, and consider the evolution of a small *localized* disturbance, which can be expressed as

$$h'(x,t) = \int_{-\infty}^{\infty} A(k)\, e^{ikx}\, e^{\omega t}\, dk, \tag{2.7}$$

where $h' = h-1$ and

$$A(k) = \frac{1}{2\pi}\int_{-\infty}^{\infty} h'(x',0)\, e^{-ikx'}\, dx'. \tag{2.8}$$

Here, the wavenumber $k$ and the frequency $\omega$ are now both complex. The initial disturbance $h'(x,0)$ is localized, but still long enough to satisfy the basic assumptions made in (2.1); thus one must truncate these for large enough $|k|$.

The asymptotic behaviour of the disturbance for $t\to\infty$ can be examined by deforming the contour of integration in (2.7) into the complex-$k$ plane, applying the method of steepest descent, and analysing the saddle point. If we now describe the flow in a reference frame moving at a speed $V$ downstream, the long-time complex frequency $\tilde{\omega}$ in that *moving* frame becomes, from (2.1) and (2.7),

$$\tilde{\omega} \equiv \omega + ikV = ik(V-G) + \epsilon k^2\left(\frac{2G^2}{15} - Sk^2\right). \tag{2.9}$$

The saddle point is that $k$, $k = k_s$, where

$$\frac{d\tilde{\omega}}{dk} = i(V-G) + 4\epsilon k\left(\frac{G^2}{15} - Sk^2\right) = 0. \tag{2.10}$$

The linear growth rate of the disturbance is given by the real part $\mathrm{Re}(\tilde{\omega})$, and this will reach its maximum when $V = G$ (see Huerre & Monkewitz 1990). It will be zero at the upstream and downstream edges of the localized disturbance. Whether there is absolute or convective instability can then be determined by examining the sense of the velocity, $V_{up}$, of the upstream edge: if $V_{up} < 0$ ($> 0$), then the instability is absolute (convective). For example, if $V_{up} > 0$, the disturbance is moving downstream and an arbitrary fixed $X$-location will become free of disturbance as $t\to\infty$.

The present analysis is asymptotically valid only when $G - V = O(\epsilon)$, since then $k_s$, given by (2.10), is of unit order. Thus, this analysis determines whether there is absolute or convective instability for long waves and holds, as long as $G$ is not too large and $S$ is not too small.

Figure 1 shows the growth rate $\mathrm{Re}(\tilde{\omega})$ versus $V$ for $S = 5$, $\epsilon = 0.1$, and four different values of $G$. For each case the maximum growth rate occurs at $V = G$, as discussed above. At this maximum, the $k_s$ at the saddle point is real and equals $k_M$. This point is bracketed by the speeds of the up- and downstream edges. In all cases shown, $V_{up}$ is positive, which shows that the instability is convective whenever long-wave theory applies.

In figure 2, the location of saddle points are plotted in the complex-$k$ plane for

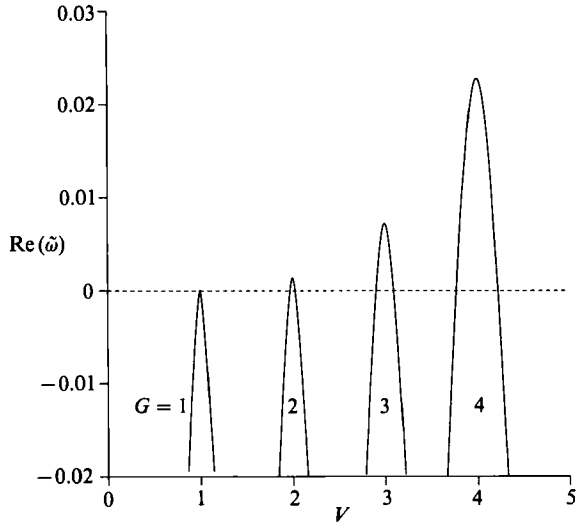


FIGURE 1. Growth rate of disturbance in a reference frame moving at speed $V$ downstream; $S = 5$, $\epsilon = 0.1$.

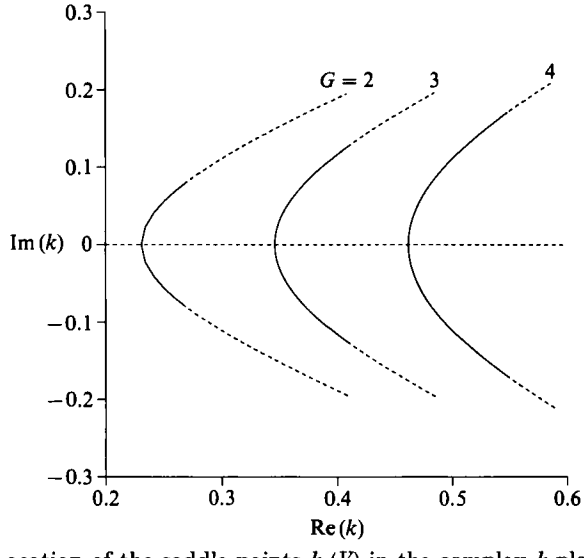


FIGURE 2. Location of the saddle points $k_s(V)$ in the complex-$k$ plane; $S = 5$, $\epsilon = 0.1$.

several values of $G$. The solid and dotted parts of the curves represent, respectively where Re ($\tilde{\omega}$) is positive and negative. The boundary between the solid and dotted parts located in the lower half-plane corresponds to $V = V_{up}$. The noses of the curves are always located on the real axis and are given by $k = G/(15S)^{\frac{1}{3}}$.

### 2.2. *Nonlinear saturation*

The nonlinear evolution of the two-dimensional waves depends strongly on the initial wavenumber $k$. As shown by Lin (1969) and Gjevik (1970), among others, there exists a value of $k_s$ such that when $k_s < k < k_c$, the flow is supercritically stable and nonlinear equilibration occurs after the initial linear instability. When $0 < k < k_s$, on the other hand, nonlinearity promotes the instability, and the saturation does not

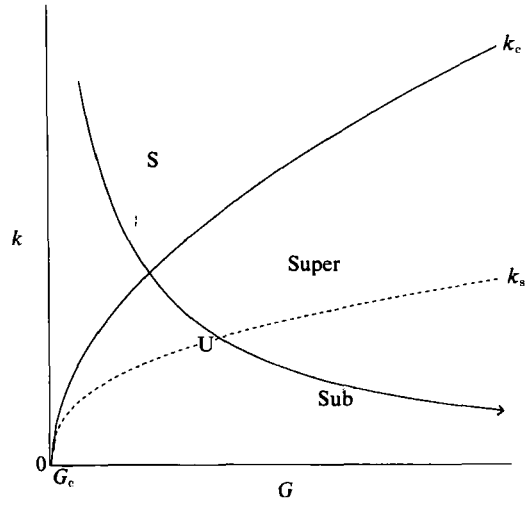


FIGURE 3. Linear/nonlinear stability diagram: S, linearly stable region; U, linearly unstable region; Super, supercritically unstable region; Sub, subcritically unstable region; line with arrow, fixed linear frequency $kG$.

occur (subcritical bifurcation) at least within the range of validity of the equation. Figure 3 shows the corresponding linear/nonlinear stability diagram. The critical Reynolds number $G_c$ is zero here because the layer is vertical. The curve with the arrow indicates a trajectory in which the linearized frequency $kG$ is fixed as $G$ is increased (see (2.5); it shows that if we lock the frequency of a wave generator, various regions can be reached by changing the Reynolds number.

In the supercritical region, the evolution can be well approximated by the fundamental wave and its few lowest harmonics:

$$h(x,t) = \sum_{n=0}^{N} A_n(t)\,\mathrm{e}^{\mathrm{i}knx} + \text{c.c.}, \tag{2.11}$$

where c.c. denotes complex conjugate and $A_0 = 1$. We follow Gjevik (1970) and set $N = 2$ in (2.11) to obtain a minimal representation; after substituting into (2.1), we obtain

$$\dot{A}_1 = \alpha_1 A_1 + \beta_1 A_1^* A_2 + \gamma_1 |A_1|^2 A_1 + 2\gamma_1 |A_2|^2 A_1, \tag{2.12}$$

$$\dot{A}_2 = \alpha_2 A_2 + \beta_2 A_1^2 + 2\gamma_2 |A_1|^2 A_2 + \gamma_2 |A_2|^2 A_2, \tag{2.13}$$

where the dot denotes time derivative, superscript * denotes complex conjugate, and the coefficients $\alpha_i$, $\beta_i$ and $\gamma_i$ $(i = 1, 2)$ are listed in Appendix A. As shown by Gjevik (1970), non-trivial steady solution ($|\dot{A}_1| = |\dot{A}_2| = \dot{\phi} = 0$) exist when

$$(2G^2/15 - k^2 S)\,(2G^2/15 - 4k^2 S) < 0, \tag{2.14}$$

or equivalently $k_s < k < k_c$, where $\phi(t)$ is the phase difference between the two modes. The upper bound for the inequality, $k_c = 2G^2/(15S)$, is the cutoff wavenumber from the linear theory, and the lower bound, $k_s = \frac{1}{2}k_c$ determines the nature of the subsequent nonlinear evolution. The corresponding free-surface configuration, steady in a reference frame $x'$ moving with a nonlinear phase velocity $c$, can be expressed as

$$\bar{h}(x') = 1 + 2[|A_1| \cos(kx') + |A_2| \cos(2kx' + \phi)], \tag{2.15}$$

where $c$, $|A_n|$, $\phi$ are given in Appendix B.

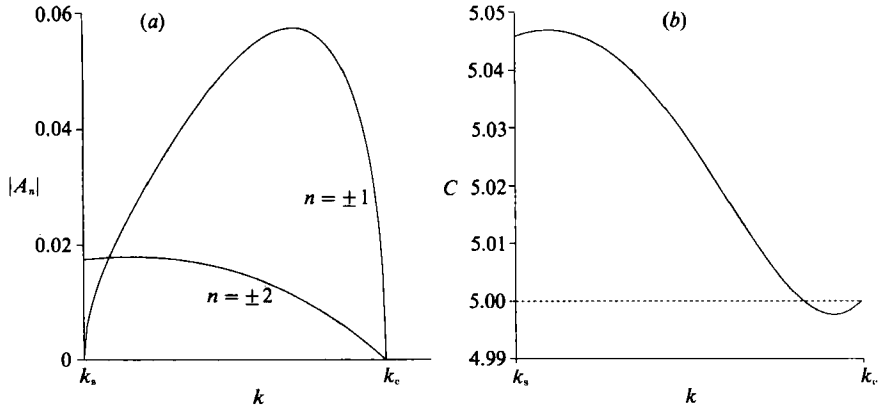


FIGURE 4. Saturated nonlinear two-dimensional permanent waves obtained from the truncated system (2.11) with $N = 2$ when $G = 5$, $T = 1$, and $\epsilon = 0.1$: (*a*) magnitudes of modes $A_{\pm 1}$ and $A_{\pm 2}$ versus the wavenumber $k$; (*b*) nonlinear phase speed $c$ versus the wavenumber $k$.

Figure 4 shows some of the features of the permanent wave (2.15) when $G = 5$, $T = 1$, and $\epsilon = 0.1$. In figure 4(*a*), the magnitudes $|A_n|$ are plotted for $k_s < k < k_c$. As $k$ is decreased from $k_c$, the amplitude $|A_1|$ of the fundamental increases rapidly and reaches a maximum before $k$ reaches $k_M$. The magnitude $|A_2|$ of the harmonic increases monotonically and becomes dominant near $k = k_s$. However, the accuracy of the truncated-equations analysis deteriorates near $k_s$ for the reasons stated below and so the diagrams in Figure 4 should be interpreted with care. In fact, the system (2.12), (2.13) is valid only when $|A_1| \gg |A_2|$, and this ceases to hold near $k = k_s$. Figure 4(*b*) shows the phase speed $c$ of the finite-amplitude permanent wave. For $G = 5$ the linear theory gives that the phase speed is 5 (twice the maximum speed of the fluid in its basic state), and is indicated by the dotted horizontal line in the figure. Near $k = k_c$ the nonlinear phase speed decreases as $k$ is decreased, and reached a minimum, after which it increases and reaches a maximum near $k_s$. The decrease of the phase speed near $k_c$ is consistent with the higher-order (in $\epsilon$) analyses of Lin (1969) and Chang (1989).

Another way to obtain the finite-amplitude permanent wave and confirm the nonlinear saturation is to pose an initial-value problem in a periodic domain and integrate the evolution equation (2.1) numerically. Joo *et al.* (1991), for example, have done several calculations for different values of $k$. When $k$ is sufficiently close to $k_c$, the nonlinear equilibration occurs and the permanent wave is well described by (2.15). However, as $k$ gets closer to $k_s$, higher harmonics than those retained in (2.15) become important and the equilibrated state, if any, cannot be represented by (2.15). In fact, very close to $k_s$, the permanent wave takes the form of a localized, periodic wave, which is rather broadbanded. Moreover, as discussed by Pumir *et al.* (1983), when $G$ is larger than a certain critical value, the saturation near $k_s$ ceases to exist; the criterion (2.14) becomes a poor estimate as $G$ increases. The actual $k_s$ obtained through computation (large $N$) would necessarily be larger than that from (2.14) except near the critical Reynolds number, here $G_c = 0$.

Figure 5 shows the evolution of each mode for three different values of $k$ when $G = 5$, $T = 1$, $\epsilon = 0.1$ ($k_M = 0.99$). A Fourier-spectral method is used in a periodic domain $[0, 2\pi/k]$ with $N = 16$ for $k = 1.2$ and $k = 1$ and with $N = 32$ for $k = 0.8$. As shown in figure 5(*b*) for $k = 1$, two different initial disturbance amplitudes are used to show that the fate of the disturbance is not sensitive to initial amplitude. For all cases, the primary instability near $t = 0$ and subsequent nonlinear saturation are

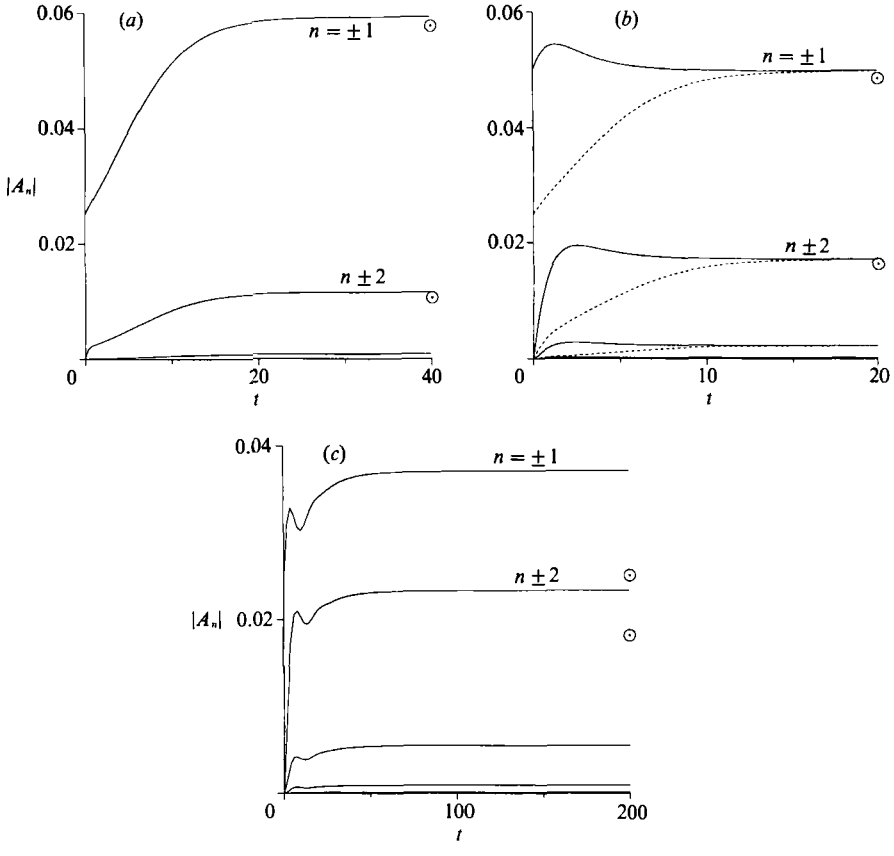


FIGURE 5. Evolution of Fourier spectrum showing the nonlinear saturation of linearly unstable waves. Final states obtained from the truncated system ($\odot$) are shown for comparison. $G = 5$, $T = 1$, $\epsilon = 0.1$, and the disturbance wavenumbers ($k_M \approx 1$): (*a*) $k = 1.2$; (*b*) $k = 1$; (*c*) $k = 0.8$.

seen. For $k = 1.2$ and 1, the equilibrated state can, indeed, be well described by the truncated series (2.15), as indicated in the figure. For $k = 0.8$, the truncated system (2.12), (2.13) appears to underestimate nonlinear interactions, and the modes predicted by (2.15) are substantially smaller in magnitude. Therefore, (2.15) can be a useful measure of the equilibrated state sufficiently far from $k_s$. In the following three-dimensional linear stability analysis, (2.15) will be used as the basic state, whereas in the full nonlinear computations in §4, the base state will be obtained through spectral computations, as in figure 5.

## 3. Secondary three-dimensional spatially synchronous instability

We now study the stability of the two-dimensional permanent waves to infinitesimal three-dimensional disturbances. The basic state $\bar{h}$ for this secondary instability is steady in a frame moving with the nonlinear phase speed $c$. Therefore, if we rewrite (2.1) using a coordinate transformation $x' = x - ct$, the resulting equation allows a solution of the form

$$h = \bar{h}(x') + \delta[H(x')\,\mathrm{e}^{\mathrm{i}ly+\sigma t} + \text{c.c.}], \tag{3.1}$$

where $\frac{1}{2}\delta$ is the initial small amplitude, $l$ is the spanwise wavenumber, and $\sigma$ is the linear growth rate of the three-dimensional disturbance.

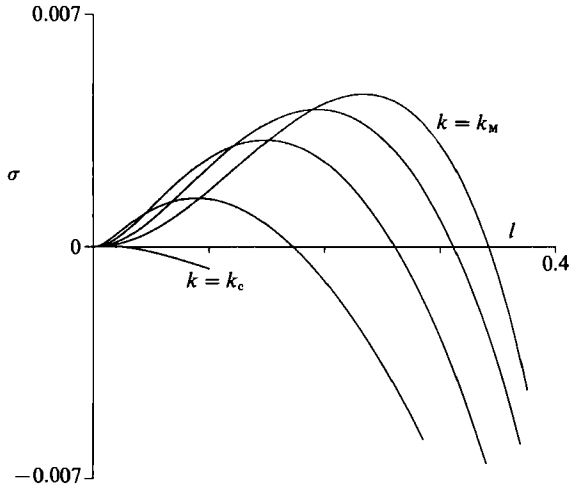


FIGURE 6. Growth rates of the three-dimensional disturbance versus the spanwise wavenumber $l$, showing the secondary instability when $G = 5$, $T = 1$, and $\epsilon = 0.1$. The streamwise wavenumbers are, from right to left, $k = 1$, 1.1, 1.2, 1.3, $k_c$.

We substitute (3.1) into (2.1) and linearize in $\delta$ to obtain the following linear eigenvalue problem for $H(x')$ and $\sigma$:

$$\bar{h}^3 H^{\mathrm{iv}} + 3\bar{h}^2\bar{h}' H''' + \left(\frac{2G^2}{15S}\bar{h}^3 - 2l^2\right)\bar{h}^3 H'' + \left(3\bar{h}^2\bar{h}''' + \frac{8G^2}{5S}\bar{h}^5\bar{h}' + \frac{G}{\epsilon S}\bar{h}^2 - \frac{c}{\epsilon S} - 3l^2\bar{h}\bar{h}'\right)H'$$
$$+\left[3(\bar{h}^2\bar{h}''')' + \frac{4G^2}{5S}(\bar{h}^5\bar{h}')' + \frac{2G}{\epsilon S}\bar{h}\bar{h}' + l^2\bar{h}^3 + \frac{\sigma}{\epsilon S}\right]H = 0, \quad (3.2)$$

where prime denotes differentiation with respect to $x'$. The coefficients in (3.2) are periodic in $x'$, and the Floquet theorem allows us to express the solution of (3.2) as

$$H = \mathrm{e}^{\mathrm{i}\lambda x'} \sum_{n=-N}^{N} c_n \mathrm{e}^{\mathrm{i}knx'}, \quad (3.3)$$

where the function represented by the finite Fourier sum has the same period $2\pi/k$ as the coefficients of (3.2) and $\lambda$ is the Floquet exponent. If $\lambda = 0$, the eigenfunction $H$ has the same period as the base state $\bar{h}$, and we are led to study *synchronous* solutions with wavelength $2\pi/k$, as performed by Orszag & Patera (1983) for wall-bounded shear flows. If $\lambda = \pm\frac{1}{2}$, the principal *subharmonic* solutions can be studied, as Herbert (1983) examined for plane channel flow. In the present study, we set $\lambda = 0$ in order to single out the three-dimensional synchronous instability.

We set $\lambda = 0$, and take $N = 2$ and $c_{-n} = c_n^*$ in (3.3). The truncation is consistent with that of $\bar{h}$, and by taking $H$ to be real, $\sigma$ becomes real. This phase-locking of the three-dimensional waves with the two-dimensional field is also used by Orszag & Patera (1983) and can be easily seen in the computations. We substitute (3.3) into (3.2) to obtain a $5 \times 5$ real-eigenvalue matrix problem. The eigenvalues $\sigma$ are then obtained from the resulting fifth-degree characteristic equation.

In figure 6, growth rates for five different values of $k$ are plotted against the spanwise wavenumber $l$ when $G = 5$, $T = 1$, and $\epsilon = 0.1$. The streamwise wavenumber $k$ determines the basic state $\bar{h}$ as illustrated in figure 4. The figure shows that two-dimensional permanent wave are unstable to three-dimensional dis-

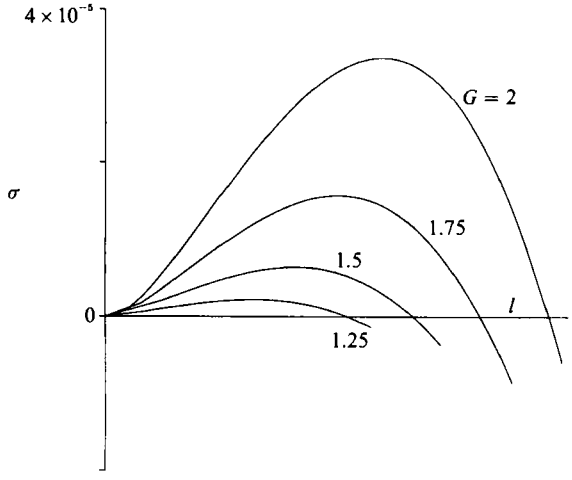


FIGURE 7. Growth rates of the three-dimensional disturbance versus the spanwise wavenumber $l$ when $T = 1$, $\epsilon = 0.1$, $k = k_M$, and at the Reynolds numbers shown.

turbances when the spanwise wavenumber is small enough. The secondary instability appears for long cross-stream waves and surface tension provides a short-wave cutoff, as in the primary instability. The spanwise cutoff wavenumber $l_c$ decreases monotonically toward zero as $k$ approaches $k_c$. Neither $l_c$ nor the maximum growth rate reaches an extremum near $k = 1.2$, at which $\bar{h}$ has maximum amplitude. It appears that the secondary instability is always present and does not involve a threshold amplitude of the basic state. If we allow higher-order nonlinear interactions by taking larger $N$ in (2.11) and (3.2), the growth rate, and thus $l_c$, tend to increase. This underestimation of instability by a truncated system is also observed by Orszag & Patera (1983) in their shear-flow instability theory.

In figure 7, growth rates are plotted for different values of $G$ when $T = 1$, $\epsilon = 0.1$, and $k = k_M = G^{\frac{5}{6}}/\sqrt{15}$. As the mean layer thickness (or $G$) decreases, the driving force for instability weakens, and the growth rate and $l_c$ decrease. The critical value of $G$ for the secondary instability appears to be zero, as for the primary instability, so that there is an unconditional instability of the two-dimensional wave.

In figure 8, the cutoff wavenumber $l_c$ of the secondary instability is plotted against $G$, while $T = 1$, $\epsilon = 0.1$, and $k = k_M$. The basic state $\bar{h}$, therefore, is the two-dimensional permanent wave equilibrated from disturbances with the maximizing wavenumber of the linear theory, i.e. (2.15) with $k_M$. As $G$ increases, $l_c$ increases, as seen also in figure 7. For moderate $G (G < 7)$, the increase is almost linear. A straight line $l_c = 0.072G$ is plotted for comparison. For large $G$, the increase becomes strongly nonlinear. When $T$ is fixed at a constant value, the cutoff wavenumber $k_c$ for two-dimensional disturbance is proportional to $G^{\frac{5}{6}}$. Therefore, the ratio $l_c/k_c$ would increase weakly as $G$ increases.

In figure 9($a$) the maximum growth rate $\sigma_M$ of the secondary instability is plotted when $T = 1$, $\epsilon = 0.1$, and $k = k_M$. For small $G$, the rate of increase of $\sigma_M$ is small, but as $G$ becomes large, the rate of increase becomes very large, showing a strong dependence of the secondary instability on the layer thickness. For fixed $T$, the maximum growth rate $\Gamma_M$ of the two-dimensional primary instability is proportional to $G^{\frac{11}{3}}$. The ratio $\sigma_M/\Gamma_M$ of the maximum growth rate of the secondary instability to that of the primary instability is plotted in figure 9($b$). It is seen that the relative growth rate of the secondary instability is small but increases with $G$.

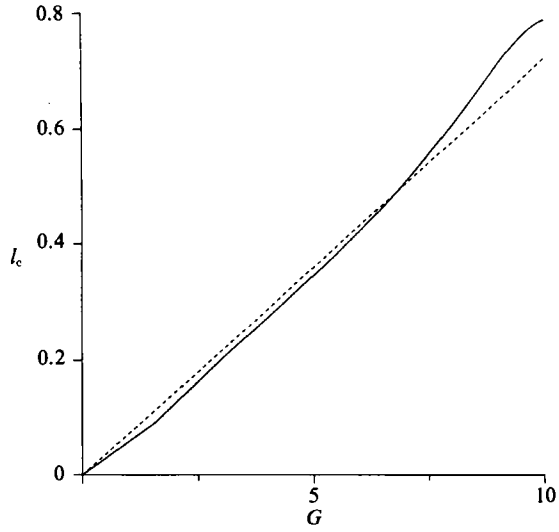


FIGURE 8. Cutoff disturbance wavenumber $l_c$ of the secondary three-dimensional instability with $k = k_M$ and $T = 1$. The broken line is for reference, $l_c = 0.072G$.

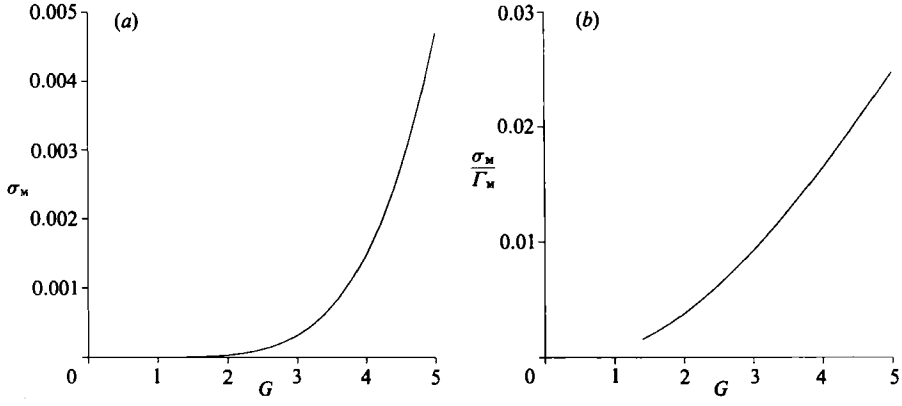


FIGURE 9. Maximum growth rate $\sigma_M$ of the three-dimensional instability with $k = k_M$ and $T = 1$: (*a*) $\sigma_M$ *vs.* $G$; (*b*) $\sigma_M/\Gamma_M$ *vs.* $G$, where $\Gamma_M$ denotes maximum growth rates of the two-dimensional surface-wave instability.

## 4. Computations of three-dimensional layers

In this section, we pose a series of initial-value problems that probes the nonlinear evolution of three-dimensional layers as related to the secondary instability identified in §3. The evolution equation (2.1) is integrated temporally by a Hamming modified predictor–corrector method with a Fourier spectral method for spatial derivatives. The initial time marching is done by a fourth-order Runge–Kutta method, and the maximum $\Delta t$ is set to $10^{-4}$ while the actual $\Delta t$ is adjusted automatically to satisfy an absolute error bound set to $10^{-11}$. The spatial resolution is secured by taking a minimum collocation of $16 \times 16$.

The boundary conditions are periodicity on a domain $0 \leqslant x \leqslant 2\pi/k$ and $0 \leqslant y \leqslant 2\pi/l$. We use the following two sets of initial conditions:

(i) a two-dimensional permanent wave plus a small spanwise perturbation,

$$h = \bar{h}(x'; k) - \delta_1 \cos(ly); \tag{4.1}$$

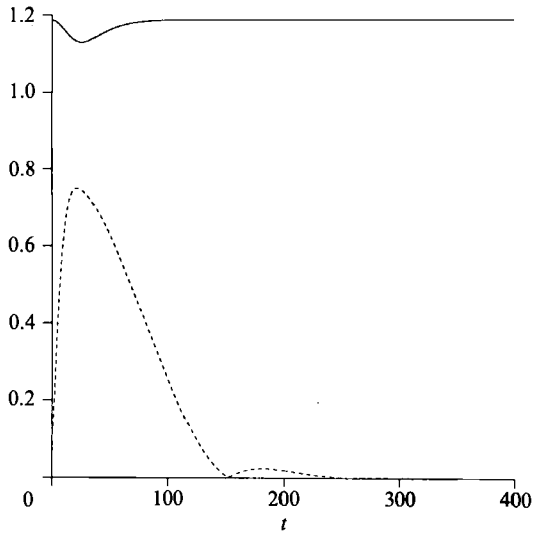


FIGURE 10. Evolution of the norms $N_x$ (——) and $N_y$ (– – –) with the initial condition (4.1) when $G = 5$, T = 1, $\epsilon = 0.1$, $k = 1$, and $l = 0.5$: a three-dimensionally stable evolution.

(ii) a small harmonic disturbance to the planar interface in both streamwise and spanwise directions,

$$h = 1 - \delta_2 \cos(kx) - \delta_2' \cos(ly). \tag{4.2}$$

Here, $\delta_1 = 0.01$ and $\delta_2 = \delta_2' = 0.05$. The initial condition (4.1) allows us to examine the secondary instability and study its nonlinear behaviour. The basic state $\bar{h}$, as shown in figure 5, is obtained from spectral computation, so that we can examine the instability closer to $k_s$ than allowed by the series truncation of §3. The initial condition (4.2) provides insight into the formation of three-dimensional structures for given comparable perturbations in $x$ and $y$.

### 4.1. *Case 1*

We first experiment with the initial condition (4.1) for $G = 5$, $T = 1$, and $\epsilon = 0.1$. We take $k = 1$ and different values of $l$; note that the truncated system gives $l_c \approx 0.35$. The Fourier spectrum of the basic state $\bar{h}$ has already been illustrated in figure 5(*b*).

In figure 10, we take $l = 0.5$, which lies outside of the unstable range in figure 6. Capillary forces will suppress the spanwise perturbation, and thus the two-dimensional permanent wave $\bar{h}$ will be recovered. This stable evolution is illustrated by plotting two norms, $N_x$ and $N_y$, which measure the streamwise and spanwise components of the total wave energy, respectively:

$$N_x(t) = \frac{l}{2\pi} \int_0^{2\pi/l} \left( \sum_{n=1}^{N} a_n^2 \right)^{\frac{1}{2}} \mathrm{d}y, \tag{4.3}$$

$$N_y(t) = \frac{k}{2\pi} \int_0^{2\pi/k} \left( \sum_{m=1}^{M} b_n^2 \right)^{\frac{1}{2}} \mathrm{d}x, \tag{4.4}$$

where the Fourier spectra $a_n$ and $b_m$ are obtained from

$$h(x,y,t) = \sum_{n=0}^{N} a_n(y,t)\, \mathrm{e}^{\mathrm{i}knx} + c.c. = \sum_{m=0}^{M} b_n(x,t)\, \mathrm{e}^{\mathrm{i}lmy} + \mathrm{c.c.} \tag{4.5}$$

When $t = 0$, the norms in figure 10 indicate that a small spanwise disturbance (or $N_y$)

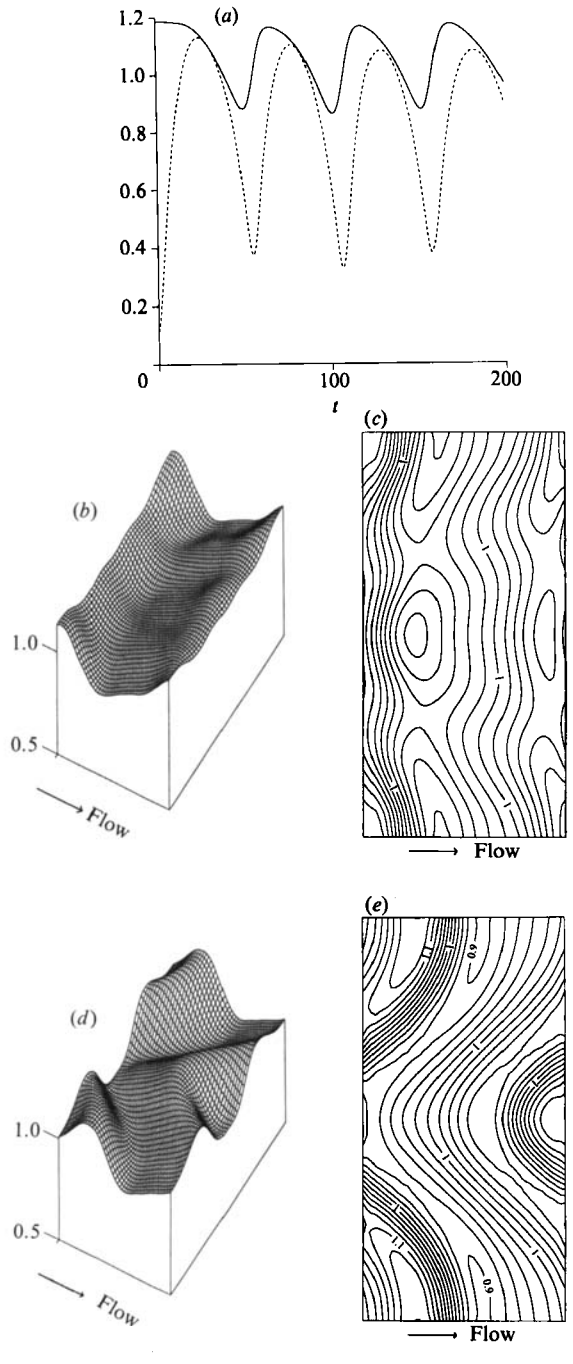


FIGURE 11. A three-dimensionally unstable evolution for initial condition (4.1): $G = 5$, $T = 1$, $\epsilon = 0.1$, $k = 1$, and $l = 0.25$. (*a*) Evolution of the norms $N_x$ (——) and $N_y$ (– – –); (*b*) configuration of the free surface at $t = 158$; (*c*) contours of constant thickness at $t = 158$; (*d*) configuration of the free surface at $t = 183$; (*e*) contours of constant thickness at $t = 183$.

is added to the larger two-dimensional basic state (or $N_x$). Initially, $N_y$ and $N_x$ show, respectively, substantial increase and decrease from their initial states. However, $N_y$ eventually decays to zero, while $N_x$ increases and recovers its initial value; the two-dimensional permanent wave is recovered. The oscillations of $N_y$ suggests that the flow is not monotonically stable. This transiency stems from the strong thickness-dependence of the local phase speed. The spanwise disturbance imposed on the saturated two-dimensional wave that travels with constant phase speed (no streamwise variation) induces the spanwise variation of the phase speed, resulting in the tendency toward three-dimensional patterns. When $l > l_c$, however, the surface tension eventually damps the spanwise perturbation. Thus for sufficiently larger $l$ the flow becomes monotonically stable, whereas for $l$ closer to $l_c$ the transiency is more pronounced.

In figure 11, the spanwise wavenumber $l = 0.25$, which lies inside the unstable region in figure 6. Small initial disturbance will grow, giving rise to three-dimensional structures. The norms plotted in figure 11 (*a*) show the initial three-dimensional instability, consistent with the analysis in the previous section, followed by a series of growth/decay. These oscillations are reminiscent of the recurrence of the Fermi–Pasta–Ulam type (Fermi *et al.* 1955), an example of which is shown numerically by Yuen & Ferguson (1978) in their study of the nonlinear Schrödinger equation associated with Benjamin–Feir instability. The system considered in figure 11 is dissipative, and true 'recurrence' does not occur. Near the maxima in $N_y$, the surface wave is strongly three-dimensional, whereas near the minima, it is weakly so. Near the minima, the crests and the troughs of the spanwise wave component are lined up at about the same streamwise location, as shown in figure 11 (*b*, *c*). However, the crests travel faster downstream making the surface shape more three-dimensional until $N_y$ reaches a maximum, as in figure 11 (*d*, *e*). The crests then start to catch up with the troughs downstream, and nearly line up with them near the next minimum of $N_y$. Other calculations (not shown in the figure) show that the temporal oscillation period (locally) of $N_y$ decreases with the increase of the disturbance amplitude $\delta_1$.

The computation of layers with sufficiently long spanwise disturbances shows the secondary three-dimensional instability and subsequent nonlinear evolutions. The three-dimensional mode grows initially, but stays bounded at least within the integration time performed (e.g. up to $t = 800$ for figure 11). The surface configuration evolves into a strongly three-dimensional pattern, and then into a more weakly three-dimensional one, followed by an irregular 'recurrence' between these two patterns. This process continues without reaching any well-defined state, and there is no indication that the instability leads to a three-dimensional saturation.

### 4.2. *Case 2*

We now use the initial condition (4.2) and study the nonlinear evolution of disturbances that are harmonic in both the streamwise and spanwise directions. We set $G = 5$, $T = 1$, and $\epsilon = 0.1$, as before.

In figure 12, $k = 1$ and $l = 0.5$. The wavenumbers are identical to those in figure 10. The evolution of the two norms are plotted up to $t = 350$. Initially $N_x$ and $N_y$ are equal in magnitude because the amplitudes $\delta_2$ and $\delta_2'$ are equal. As the fluid flows downstream, the wave amplitude grows due to the primary surface-wave instability. As in figure 10, the spanwise wavenumber is larger than $l_c$ but not large enough for the capillary forces to cause monotonic decay of spanwise modes. Accordingly, both $N_x$ and $N_y$ increase with time until they reach maxima at about $t = 13$, after which oscillatory behaviour is observed. Eventually $N_x$ increases to its value for the two-

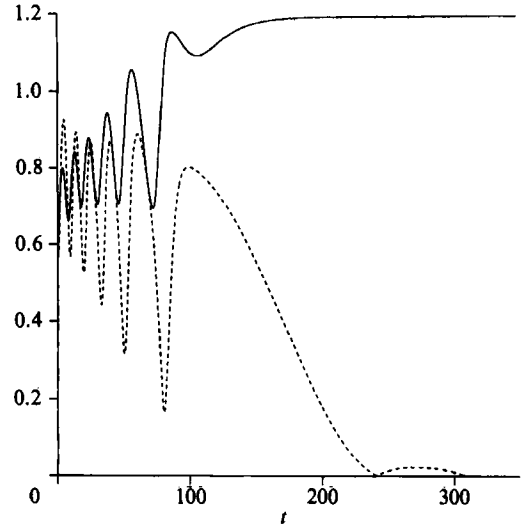


FIGURE 12. Evolution of the norms $N_x$ (——) and $N_y$ (– – –) with the initial condition (4.2) when $G = 5$, $T = 1$, $\epsilon = 0.1$, $k = 1$, and $l = 0.5$.

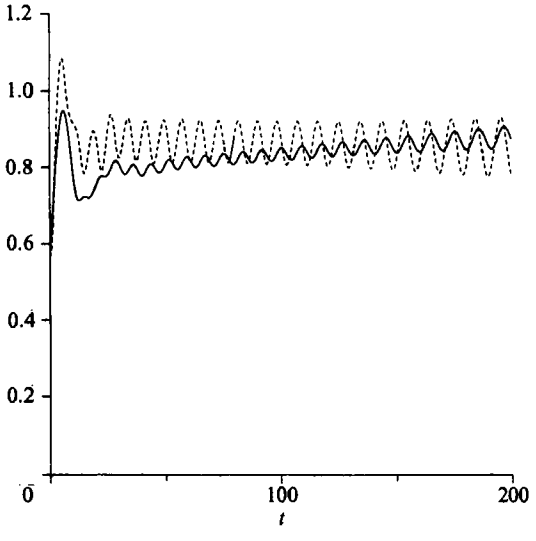


FIGURE 13. Same as figure 12 but when $l = 0.25$.

dimensional equilibrated state, while $N_y$ decays to zero, resulting in the same purely two-dimensional permanent wave as in figure 10. The two different initial conditions lead to identical equilibrated states.

Figure 13 shows the evolution of the two norms up to $t = 200$ when $k = 1$ and $l = 0.25$. The wavenumbers are identical to those in figure 11, in which the secondary instability is exhibited. For small time, the wave amplitude grows due to the primary surface-wave instability. The spanwise wavenumber is small enough ($l < l_c$), so that the three-dimensional instability is present. The norm $N_x$ also oscillates but continues to grow toward the value for saturation, shown in figure 5(*b*). In the subsequent evolution, both $N_x$ and $N_y$ are bounded, but do not show any equilibration to steady or periodic states up to $t = 400$.

The computations of three-dimensional layers with the initial condition (4.2) show the two-dimensional and the three-dimensional instabilities. When the spanwise

wavenumber is large, only the two-dimensional instability is present. The initial three-dimensional disturbance thus develops into the same two-dimensional permanent wave as that which evolves from the initial condition (4.1), if identical streamwise wavenumbers are used. When the spanwise wavenumber is small enough, a three-dimensional state will result. As in Case 1, no equilibration to a three-dimensional permanent wave is found.

### 4.3. *Case 2 for* $k < k_s$

In this case, we use streamwise wavenumbers that are smaller than the two-dimensional saturation value $k_s$; two-dimensional equilibration does not occur. The evolution is again very much dependent upon the spanwise wavenumber $l$. If $l$ is large, the initial three-dimensional disturbance will become two-dimensional, giving rise to the aforementioned tendency toward wavebreaking or unbounded growth. If $l$ is sufficiently small, the disturbance will stay three-dimensional. In this case, the amplitude and the local slope of the disturbance stay bounded, but the evolution is irregular, showing no indication of equilibration to any permanent states.

## 5. Concluding remarks

In the present study, we have tried to understand the complicated behaviour of a thin three-dimensional viscous layer falling down a *vertical* plane by studying the long-wave evolution equation of Benney type. Relatively small Reynolds numbers and relatively large surface tensions are posed as illustrative cases for the dynamics.

As the fluid flows downstream, the surface-wave instability sets in and a wave motion is exhibited at the interface. Owing to the capillary stabilization of short waves, the surface waves that appear are very long compared to the layer thickness. The linear analysis of this surface-wave instability shows that two-dimensional (transverse) waves are preferred. It also shows that for the *thin* layers that we study with realistically large surface tension, the instability is convective. The nonlinear analyses and computations show that the fate of a two-dimensional wave depends strongly upon its wavelength. When the wave is short enough ($k_s < k < k_c$), it can develop into a permanent wave as it flows downstream. On the other hand, when the wave is very long ($k < k_s$), the nonlinear interactions promote the growth, and an incipient wavebreaking or a catastrophic growth may be encountered.

The subcritical behaviour that occurs for $k < k_s$ cannot be adequately described by the evolution equation (2.1), because the long-wave approximation is violated as the wavenumber spectrum broadens. The incipient wavebreaking and the catastrophic growth obtained via the evolution equation may not be observed if the full Navier–Stokes equation is considered. Using a spectral-element method, Ho & Patera (1991) integrated the Navier–Stokes equation, and obtained equilibrated wavetrains with $k < k_s$. The Reynolds number considered is much larger than that in the present study, and a specific nonlinear initial state is used in obtaining the permanent wave.

The two-dimensional equilibrated layers that result for $k_s < k < k_c$ are susceptible to a secondary three-dimensional instability. When one considers spatially synchronous instabilities and the streamwise wavenumber $k$ is sufficiently close to $k_c$, the two-dimensional wave can be described by a truncated Fourier series, and a linear analysis can be carried out for the secondary instability. This linear stability analysis of the truncated system gives a spanwise cutoff wavenumber and maximum growth rate that are smaller than those for the two-dimensional instability and

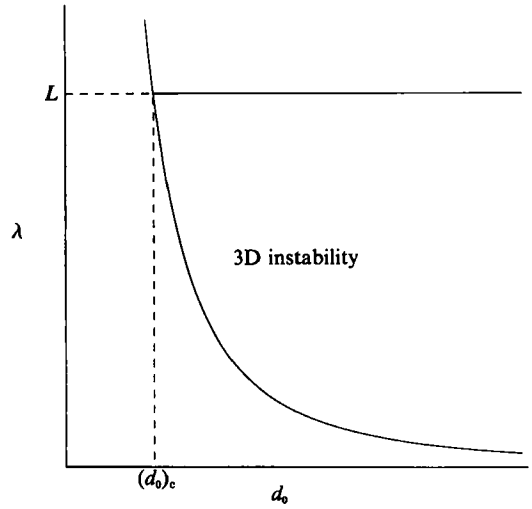


FIGURE 14. Critical wavelength $\lambda$ for the three-dimensional instability versus mean layer thickness $d_0$. $L = 2\pi(R+d_0)$, where $R$ is the radius of a cylinder.

increase with the Reynolds number. Unlike other spatially synchronous secondary instabilities that appear on a rapid convective timescale in shear flows with large Reynolds number, the present secondary instability is viscous in nature, as in the primary surface-wave instability. At least for vertical layers, the instability does not require a threshold amplitude, so that the three-dimensional instability is always present.

The nonlinear evolution of layers subject to the three-dimensional instability is studied by numerically integrating the evolution equation (2.1). It also relaxes the restriction on $k$, imposed in the truncated system. The unstable modes stay bounded, but there is no indication of three-dimensional saturation. Other computations with different initial conditions show highly irregular nonlinear behaviour when the spanwise wavenumber is small enough to make the two-dimensional wave unstable.

The three-dimensional instability identified in the present study seems at least qualitatively related to a recent experimental observation of Lacy *et al.* (1991). They examined thin viscous films flowing down a vertical cylinder, and noted that the film that has a two-dimensional ring structure that becomes three-dimensional further downstream as the ring distorts, with some portions of the ring falling more rapidly. This transition to three-dimensional waves far downstream from the wave inception has also been observed in many earlier studies including that of Alekseenko *et al.* (1985), who reported that two-dimensional waves soon become three-dimensional.

The secondary three-dimensional instability studied above applies to layers on an infinite plane. If a layer flows down a vertical cylinder, a geometrical constraint is imposed on the disturbance wavelength. As the layer thickness is decreased, longer disturbance is required for the instability to occur, as shown in figure 8. On the cylindrical surface, the wavelength cannot exceed the circumferential length $L = 2\pi(R+d_0)$, where $R$ is the radius of the cylinder and $d_0$ is again the mean thickness of the layer. If we assume that the cutoff wavenumber decreases linearly with the Reynolds number, in view of figure 8, it is deduced that the dimensional wavelength $\lambda$ for the three-dimensional instability is proportional to $1/d_0^2$. Therefore, as shown in figure 14, for a fixed radius $R$ there is a critical thickness $(d_0)_c$ below which no three-dimensional instability can be present. In the experiment of Lacy *et al.* (1991),

the radius $R = 50.8$ mm ($L \approx 325$ mm) and the mean layer thickness $d_0$ is of the order of 1 mm. If the surface tension of the glycerine–water–NaOH solution is assumed to be that of pure water, the estimated critical thickness $(d_0)_c$ is about 0.01 mm, which is much smaller than a typical $d_0$ used in the experiment. The layer thus is susceptible to the three-dimensional instability, and indeed shows three-dimensional developments as mentioned above.

The linear analysis and the computations above have been confined to layers with fixed spatial period, and the instability that we identified is spatially synchronous with the given two-dimensional wave. As a result, wave crests of consecutive waves are aligned. There may additionally be spatially subharmonic instabilities as discussed in §3. Prokopiou, Chen & Chang (1991) have identified such an instability for $l = 0$ in cases where the Reynolds number is rather large. This mode can be understood in the present case of small Reynolds number if one refers to figure 3. Given a two-dimensional wave with $k = k^{(2)}$ ($> k_s$), one can find a permanent two-dimensional wave. If one perturbs this by another two-dimensional wave with $k = \frac{1}{2}k^{(2)}$, and since $\frac{1}{2}k^{(2)} < k_s$, we have the equivalent of a two-dimensional computation of the evolution equation on a box of length $4\pi/k^{(2)}$, and we know that disturbances will display incipient breaking or catastrophic growth. In either case we know that the evolution equation is incapable of describing the long-time evolution and it remains an open question whether or not the apparent instability is a physical one. Suppose that this instability *were* physical and $l = 0$ still. Then the two-dimensional waves would modulate pairwise. If the spatially subharmonic instability were present only for $l \neq 0$, then the wave crests on alternate waves would be aligned and a herringbone pattern would be present (see Herbert 1983, figure 1 for analogous behaviour in shear flows). New, carefully controlled experiments are required to resolve this issue.

The authors gratefully acknowledge Professor S. G. Bankoff for his initial contributions and great help. They also thank Professor A. Bayliss, H.-C. Chang, and J. Gollub for valuable discussions. This work was supported by the US Department of Energy, Division of Basic Energy Sciences, through Grant no. DE FG02-86ER13641.

## Appendix A. Coefficients of equations (2.12), (2.13)

$$\alpha_1 = -ikG + k^2(\tfrac{2}{15}G^2 - k^2S), \quad \beta_1 = -2ikG + k^2(\tfrac{4}{5}G^2 - 21k^2S),$$
$$\gamma_1 = -ikG + k^2(2G^2 - 3k^2S), \quad \alpha_2 = -2ikG + 4k^2(\tfrac{2}{15}G^2 - 4k^2S),$$
$$\beta_2 = -2ikG + 2k^2(\tfrac{4}{5}G^2 - 3k^2S), \quad \gamma_2 = -2ikG + 4k^2(2G^2 - 12k^2S).$$

## Appendix B. Equations for $c, |A_n|$, and $\phi$ of two-dimensional permanent waves

$$c = \alpha_{1i} + (\beta_{1r}\sin\phi + \beta_{1i}\cos\phi)|A_2| + \gamma_{1i}|A_1|^2, \quad |A_1| = \left(\frac{\alpha_{1r}\alpha_{2r}}{\beta_{1r}\beta_{2r} - \beta_{1i}\beta_{2i} - \gamma_{1r}\alpha_{2r}}\right)^{\frac{1}{2}},$$

$$|A_2| = \frac{\alpha_{1r}(\beta_{2r}^2 + \beta_{2i}^2)^{\frac{1}{2}}}{\beta_{1r}\beta_{2r} - \beta_{1i}\beta_{2i} - \gamma_{1r}\alpha_{2r}}, \quad \phi = \arctan(\beta_{2i}/\beta_{2r}).$$

Here, subscripts r and i denote, respectively, real and imaginary parts.

## REFERENCES


ALEKSEENKO, S. V., NAKORYAKOV, V. YE & POKUSAEV, B. G. 1985 Wave formation on a vertical falling liquid film. *AIChE J.* **31**, 1446–1460.

BENJAMIN, T. B. 1957 Wave formation in laminar flow down an inclined plane. *J. Fluid. Mech.* **2**, 554–574.

BENNEY, D. J. 1966 Long waves on liquid films. *J. Maths & Phys.* **45**, 150–155.

CHANG, H.-C. 1989 Onset of nonlinear waves on falling films. *Phys. Fluids* **A1**, 1314–1327.

DEISSLER, R. J. 1987 The convective nature of instability in plane Poiseuille flow. *Phys. Fluids* **30**, 2303–2305.

FERMI, I. E., PASTA, J. & ULAM, S. 1965 Studies of nonlinear problems. In *Collected papers of Enrico Fermi* vol. II (ed. E. Segre) Document LA-1940, p. 978. University of Chicago.

GJEVIK, B. 1970 Occurrence of finite-amplitude surface waves on falling liquid films. *Phys. Fluids* **13**, 1918–1925.

HERBERT, T. 1983 Secondary instability of plane channel flow to subharmonic three-dimensional disturbances. *Phys. Fluids* **26**, 871–874.

HO, L.-W. & PATERA, A. T. 1991 A Legendre spectral element method for simulation of unsteady incompressible viscous free-surface flows. *Comput. Meth. Appl. Mech. Engng*, **80**, 355–366.

HUERRE, P. & MONKEWITZ, P. A. 1990 Local and global instabilities in spatially developing flows. *Ann. Rev. Fluid Mech.* **22**, 473–537.

JOO, S. W., DAVIS, S. H. & BANKOFF, S. G. 1991 Long-wave instabilities of heated falling films: two-dimensional theory of uniform layers. *J. Fluid Mech.* **230**, 117–146.

KAPITZA, P. L. & KAPITZA, S. P. 1949 Wave flow of thin layers of a viscous fluid. *Zh. Ekper. Teor. Fiz.* **19**, 105; also in *Collected Works*, pp. 690–709. Pergamon (1965).

KRANTZ, W. B. & GOREN, S. L. 1971 Stability of thin liquid films flowing down a plane. *Ind. Engng Chem. Fund.* **10**, 91–101.

KRISHNA, M. V. G. & LIN, S. P. 1977 Nonlinear stability of a viscous film with respect to three-dimensional side-band disturbances. *Phys. Fluids* **20**, 1039–1044.

LACY, C. E., SHEINTUCH, M. & DUKLER, A. E. 1991 Methods of deterministic chaos applied to the flow of thin wavy films. *AIChE J.* **37**, 481–489.

LIN, S.-P. 1969 Finite-amplitude stability of a parallel flow with a free surface. *J. Fluid. Mech.* **36**, 113–126.

LIN, S.-P. 1974 Finite amplitude side-band stability of a viscous film. *J. Fluid. Mech.* **74**, 417–429.

LIN, S.-P. 1983 Film waves. *Waves on Fluid Interfaces*, pp. 262–289. Academic.

LIN, S.-P. & WANG, C.-Y. 1985 Modeling wavy film flows. *Encyclopedia of Fluid Mechanics*, vol. 1, pp. 931–951.

MELKONIAN, S. & MASLOWE, S. A. 1990 Analysis of a nonlinear diffusive amplitude equation for waves on thin films. *Stud. Appl. Maths* **82**, 37–48.

ORSZAG, S. A. & PATERA, A. T. 1983 Secondary instability of wall-bounded shear flows. *J. Fluid Mech.* **128**, 347–385.

PORTALSKI, S. & CLEGG, A. J. 1972 An experimental study of wave inception on falling liquid films. *Chem. Engng Sci.* **27**, 1257–1265.

PROKOPIOU, TH., CHENG, M. & CHANG, H.-C. 1991 Long waves on inclined films at high Reynolds number. *J. Fluid. Mech.* **222**, 665–691.

PUMIR, A., MANNEVILLE, P. & POMEAU, Y. 1983 On solitary waves running down an inclined plane. *J. Fluid. Mech.* **135**, 27–50.

ROSKES, G. J. 1970 Three-dimensional long waves on a liquid film. *Phys. Fluids* **13**, 1440–1445.

YIH, C.-S. 1955 Stability of parallel laminar flow with a free surface. In *Proc. 2nd US Congr. Appl. Mech.* pp. 623–628. ASME.

YIH, C.-S. 1963 Stability of liquid flow down an inclined plane. *Phys. Fluids* **6**, 321–334.

YUEN, H. C. & FERGUSON, E. E. 1978 Relationship between Benjamin–Feir instability and recurrence in the nonlinear Schrödinger equation. *Phys. Fluids* **21**, 1275–1278.